Synthesis and Ionic Conductivity of a New Series of Modified Aurivillius Phases

Kurt R. Kendall, Julie K. Thomas, and Hans-Conrad zur Loye*

Department of Chemistry, Massachusetts Institute of Technology, Cambridge, Massachusetts 02139

Received June 1, 1994. Revised Manuscript Received November 4, 1994®

In the search for a new class of oxygen ion conductors, the new oxygen-deficient $Bi_2Sr_2M'_2M''O_{11.5}$ and the non-oxygen-deficient $Bi_2Sr_2M'_2TiO_{12}$ (M′ = Nb, Ta and M″ = Al, Ga) Aurivillius-like phases were synthesized and their ionic conductivity investigated. All of the oxygen-deficient materials showed significant oxygen ion conduction, with $Bi_2Sr_2Nb_2GaO_{11.5}$ (3.6×10^{-2} S/cm at 900 °C) exhibiting the highest conductivity. Differential thermal analysis indicated phase transitions in the oxygen-deficient materials. These transitions occurred at temperatures similar to those at which discontinuities were observed in the Arrhenius plots of the conductivity, suggesting the existence of an oxygen vacancy order–disorder transition. The electronic versus ionic contribution to the total conductivity was determined for $Bi_2Sr_2Nb_2GaO_{11.5}$, $Bi_2Sr_2Ta_2GaO_{11.5}$, and $Bi_2Sr_2Nb_2TiO_{12}$.

Introduction

Electrolyte materials for use as solid oxide fuel cells (SOFCs), oxygen sensors, oxygen pumps, and oxidation catalysts have received much attention recently as researchers try to develop materials that operate more efficiently and at lower temperatures.[1,2] The design of systems that are good oxygen ion conductors at lower temperatures will decrease the cost of operating devices that contain these materials, allowing for increased commercial applications. For example, yttria-stabilized zirconia (YSZ) is the electrolyte of choice for most SOFCs; however, because of the high activation energy of the YSZ electrolyte, the fuel cells must be operated near 1000 °C to achieve useful oxygen ion conductivity.[3–5] The high temperatures required generate several problems, including detrimental chemical reactions with the electrodes and other components of the fuel cell, incompatibility of thermal expansion coefficients, and also a shortened fuel cell life span. Because of these drawbacks of operating a fuel cell at 1000 °C, solid electrolytes that exhibit high oxygen ion conductivity and low electronic conductivity at temperatures between 600 and 800 °C or even lower are being sought as replacements.[6]

The need for lower operating temperatures is even more pressing if oxygen ion conductors are to be used as oxygen sensors, oxygen pumps, or oxidation catalysts. Desirable operating temperatures for these applications would be in the 200–400 °C range. All of these potential uses for oxygen ion conductors have created an interest in developing new classes of oxygen ion conductors that can function effectively at lower operating temperatures.

Oxygen ion conduction in solids generally occurs via a hopping mechanism whereby O^{2-} ions hop from an occupied to a vacant site.[3] YSZ, like most other materials so far studied, contains extrinsic oxygen vacancies created by doping with aliovalent cations.[7] Although this strategy frequently produces oxygen ion conduction, it has limitations. The dopant–vacancy pairs interact, and extra energy associated with overcoming this attraction causes activation energies for doped materials to increase as the dopant concentration increases. Only a small percentage of vacancies may be added before this interaction actually decreases the conductivity.[7–9] Another potential problem with doping is that after extended use at high operating temperatures, the vacancies and dopants may order or form other phases. It is therefore useful to look at other strategies for designing oxygen ion conductors, such as the synthesis of intergrowth structures that contain intrinsic oxygen vacancies.

Using this approach, we have designed new Aurivillius-like phases ($Bi_2A_{n-1}Mn_nO_{3n+3}$) that have oxygen vacancies incorporated into the perovskite layer. The Aurivillius phases,[10–12] shown in Figure 1, are layered materials with perovskite $\{A_{n-1}M_nO_{3n+1}\}^{2-}$ regions sandwiched between puckered $\{Bi_2O_2\}^{2+}$ sheets.[13,14] The new materials reported in this paper consist of intergrowths derived from the Aurivillius phase and the brownmillerite-related phases ($Sr_2Ga_2O_5$, $Sr_2Al_2O_5$). The brownmillerite phases are oxygen-deficient perovskites

* To whom correspondence should be addressed.

® Abstract published in *Advance ACS Abstracts,* December 1, 1994.

(1) Minh, N. Q. *J. Am. Ceram. Soc.* **1993**, *76*, 563–588.
(2) Di Cosimo, R.; Burrington, J. D.; Grasselli, R. K. *J. Catal.* **1986**, *102*, 234–239.
(3) Riess, I. In *Science and Technology of Fast Ion Conductors*; Tuller, H. L., Balkanski, M., Ed.; Plenum Press: New York, 1987; pp 23–50.
(4) Takahashi, T.; Iwahara, H. *Mater. Res. Bull.* **1978**, *13*, 1447–1453.
(5) Dell, R. M.; Hooper, A. In *Solid Electrolytes*; Hagenmüller, P., van Gool, W., Eds.; Academic Press: New York, 1978; pp 291–312.
(6) Hagenmuller, P. In *Superionic Solids and Solid Electrolytes*; Laskar, A. L., Chandra, S., Ed.; Academic Press: New York, 1989; pp 679–704.
(7) Kilner, J. A.; Brook, R. J. *Solid State Ionics* **1982**, *6*, 237–252.
(8) Catlow, C. R. A. In *Superionic Solids and Solid Electrolytes*; Laskar, A. L., Chandra, S., Eds.; Academic Press: New York, 1989; pp 339–379.
(9) Burggraaf, A. J.; Van Dijk, M. P.; Verkerk, M. J.; de Vries, K. J. In *Solid State Chemistry 1982. Second European Conference*; Elsevier Scientific Publishing: Veldhoven, The Netherlands, 1982; pp 185–188.
(10) Aurivillius, B. *Ark. Kemi.* **1949**, *1*, 463–480.
(11) Aurivillius, B. *Ark. Kemi.* **1949**, *1*, 499–512.
(12) Aurivillius, B. *Ark. Kemi.* **1949**, *2*, 519–527.
(13) Subbarao, E. C. *J. Am. Ceram. Soc.* **1962**, *45*, 166–169.
(14) Subbanna, G. N.; Guru Row, T. N.; Rao, C. N. R. *J. Solid State Chem.* **1990**, *86*, 206–211.

0897-4756/95/2807-0050$09.00/0

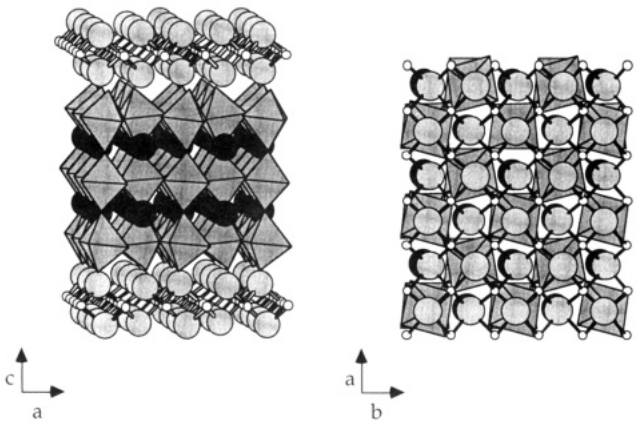

Figure 1. Structure of the Aurivillius phase $Bi_2Sr_2Nb_2TiO_{12}$ viewed in the *ac* plane and down the *c* axis. Within the puckered sheet region (shown as ball and stick) the light gray spheres represent Bi^{3+} and the white spheres O^{2-}. In the perovskitic region, the MO_6 (M = Nb, Ti) octahedra are shown as polyhedra and the dark spheres are Sr^{2+}.

with vacancy ordering along the [101] direction,[15] while in related structures the vacancies may exhibit different ordering.[16] The impetus for creating an intergrowth of both of these phases is 2-fold. First, it has been reported that Bi_2WO_6 and $Bi_2VO_{5.5}$, both $n = 1$ Aurivillius phases, exhibit high oxygen ion conductivity at low temperatures;[17–21] and second, the brownmillerite phases are known to exhibit low-temperature oxygen ion conductivity above an order/disorder transition.[22] Since the brownmillerite and perovskite structures are similar, we have been able to substitute brownmillerite–related layers for some of the perovskite layers in the structure, thereby introducing oxygen vacancies.[23] We have investigated these new materials, which consist of intergrowths between an Aurivillius phase and a brownmillerite-like phase, to develop a new class of oxygen ion conductors.

In this paper we describe the synthesis of new Aurivillius-like phases, $Bi_2Sr_2M'_2M''O_{11.5}$ (M′ = Nb, Ta, and M″ = Al, Ga), and Aurivillius phases, $Bi_2Sr_2M'_2TiO_{12}$, and the measurement of their ionic conductivity. We also report differential thermal analysis measurements which confirm the existence of phase transitions. For all of the oxygen-deficient structures, we have observed hysteresis in the Arrhenius plot of the ionic conductivity and have measured ionic conductivities as high as 3.6×10^{-2} S/cm at 900 °C for $Bi_2Sr_2Nb_2GaO_{11.5}$.

Experimental Methods

The samples were prepared by the solid-state reaction of the oxides Al_2O_3 (Johnson Matthey, 99.99%), Bi_2O_3 (Johnson Matthey, 99.99%), Ga_2O_3 (Johnson Matthey, 99.999%), Nb_2O_5 (Johnson Matthey, 99.9+%), Ta_2O_5 (Johnson Matthey, 99.9%), and TiO_2 (anatase, Aldrich, 99.9+%) and the carbonate $SrCO_3$ (Johnson Matthey, grade 1). The powders were intimately mixed by either grinding under acetone with an agate mortar and pestle or by using a micronizer (McCrone Micronizer Mill) with agate pellets and water to create a fine powder of submicron–sized particles. The powders were uniaxially pressed into either 1, 3/4, or 1/2 in. pellets under 5000 pounds. The pellets were heated slowly in air to 800 °C at 3 °C/min to convert the strontium carbonate into the oxide and to react the bismuth oxide, thus preventing melting. After several days, the samples were cooled, analyzed by powder X-ray diffraction (XRD) to determine the reaction progress, and then reground and heated until a single phase, as shown by XRD, was obtained. Usually two more heatings to 1100 °C for 3 days were required.

The polycrystalline samples were structurally characterized by XRD on a Rigaku RU300 diffractometer with Cu Kα radiation (λ = 1.541 84 Å). NBS silicon was used as an internal standard for accurate peak positions. Lattice parameters were determined using the computer software PPLP in the NRCVAX package.[24]

Simultaneous differential thermal analysis and thermogravimetric analysis (DTA-TGA) data were obtained using a TA Instruments SDT 2960. Samples were run under atmospheres of oxygen, nitrogen, and air. Performing the measurements under different atmospheres ensured that observed transitions were independent of the oxygen partial pressure. The furnace was ramped up and down at 25 °C/min. The decomposition temperatures for the different samples were also determined to help optimize the sintering conditions for the sample pellets before conductivity measurements were taken.

Prior to the conductivity measurements, the sample pellets, ≈12 mm in diameter and 5 mm in width, were sintered for 6–12 h between 1125 and 1200 °C. Several different pellet geometries were used to help deconvolute the impedance data. The faces of the sintered pellets were sanded, and platinum ink was painted onto the faces to form the electrodes. The paint was then baked onto the surface at 850 °C for 1 h. Degradation of the two platinum electrodes occurred after prolonged exposure to temperatures greater than 800 °C and, in the case of some samples, resulted in a decrease in the measured ionic conductivity.

Ac impedance measurements were carried out on sintered pellets over the frequency range 1 Hz to 5 MHz using a Solartron 1260 impedance/gain-phase analyzer interfaced to a PC computer driven by Z-plot software.[25] The ionic conductivity was measured up to 975 °C, the maximum temperature allowed by our sample holders. The samples were cycled between 300 and 975 °C in 50, 25, or 10 °C increments. The heating or cooling rates between intervals were not varied; however, the conductivity measurements were repeated using different increments. In none of the conductivity measurements did the size of the increment affect the conductivity value. The pellets were allowed to equilibrate for 4–6 h at each interval before the conductivity was measured.

The electronic versus ionic contribution to the total conductivity was determined by carrying out impedance measurements under atmospheres having different oxygen partial pressures and determining the dependence of the conductivity on the oxygen partial pressure.[26] Oxygen/argon mixtures (Matheson, certified) were used for oxygen partial pressures down to 1 ppm. For partial pressures of oxygen below 1 ppm, carbon dioxide/carbon monoxide mixtures with the balance in argon (AIRCO, certified) were used. Through the use of the equation for the Gibbs free energy, $\Delta G° = 86.81T - 282\,400$ J, for the reaction $CO + {}^1/_2O_2 \leftrightarrow CO_2$, the partial pressure of

(15) Berggren, J. *Acta Chem. Scand.* **1971**, *25*, 3616–3624.
(16) Anderson, M. T.; Vaughey, J. T.; Poeppelmeier, K. R. *Chem. Mater.* **1993**, *5*, 151–165.
(17) Yanovskii, V. K.; Voronkova, V. I.; Aleksandrovskii, A. L.; D'yakov, V. A. *Sov. Phys. Dokl. Engl. Trans.* **1975**, *20*, 306–307.
(18) Yanovskii, V. K.; Voronkova, V. I.; Roginskaya, Y. E.; Venevtsev, Y. N. *Sov. Phys. Solid State Engl. Transl.* **1982**, *24*, 1603–1604.
(19) Abraham, F.; Debreuille-Gresse, M. F.; Mairesse, G.; Nowogrocki, G. *Solid State Ionics* **1988**, *28–30*, 529–532.
(20) Sharma, V.; Shukla, A. K.; Gopalakrishnan, J. *Solid State Ionics* **1992**, *58*, 359–362.
(21) Lee, C. K.; Sinclair, D. C.; West, A. R. *Solid State Ionics* **1993**, *62*, 193–198.
(22) Goodenough, J. B.; Ruiz-Diaz, J. E.; Zhen, Y. S. *Solid State Ionics* **1990**, *44*, 21–31.
(23) Thomas, J. K.; zur Loye, H. C. *J. Am. Chem. Soc.*, submitted.
(24) NRCVAX–An Interactive Program System for Structure Analysis. Gabe, E. J.; Page, Y. L.; Charland, J.-P.; Lee, F. L.; White, P. S. *J. Appl. Crystallogr.* **1989**, *22*, 384.
(25) Scribner Associates, Charlottesville, Virginia, 1991.
(26) Tuller, H. L.; Moon, P. K. *Mater. Sci. Eng. B–Solid State M.* **1988**, *B1*, 171–191.

oxygen can be calculated.[27] This provided a range of partial pressures of 10^{-12}–10^{-22} atm of oxygen. The measurements were performed from high p_{O_2} to low p_{O_2}. The gas flow rate was kept above 150 sccm in order to ensure sufficient gas mixing and to prevent separation in the gases.[28] The oxygen partial pressure in the gas stream was measured before and after passing over the pellet using YSZ-based oxygen sensors. The presence of oxygen sensors before and after the sample allowed for confirmation of the calculated p_{O_2}. After changing the gas mixtures, the sample pellets were allowed to equilibrate for several hours before carrying out any conductivity measurements.

Results and Discussion

(a) Structure. The Aurivillius phases (Figure 1), $Bi_2A_{n-1}M_nO_{3n+3}$ (n = 1–5), consist of perovskitic $\{A_{n-1}M_nO_{3n+1}\}^{2-}$ regions sandwiched between puckered $\{Bi_2O_2\}^{2+}$ layers. Within the perovskite regions the 12-coordinate **A** site can accommodate large cations such as Bi^{3+}, K^+, Na^+, Ba^{2+}, and Sr^{2+}, while smaller cations such as Ti^{4+}, Nb^{5+}, and W^{6+} are known to fit in the octahedral **M** sites.[14,29,30] The bismuth oxide layer is much more inert with regard to substitution than the perovskite layer, with the exception of isoelectronic elements such as Pb^{2+} and Sb^{3+}, which have been substituted into the $\{Bi_2O_2\}^{2+}$ layer.[31,32] As a result, the bismuth oxide layer acts as a backbone for the structure and permits for the substitution of cations in the perovskite layer. The permissible size range of the cations in the perovskite layer is only slightly smaller than that for an unconstrained perovskite structure.[33–35] This flexibility in substitution allows for the rational manipulation of the structure to improve the ionic conductivity. Our work has examined the effect on the ionic conductivity of introducing oxygen vacancies into the structure by the addition of entire layers of oxygen-deficient perovskites.[36] This approach allows us to control the oxygen vacancy concentration and study its effect on the ionic conductivity.

The structure of the new oxygen-deficient three-layer Aurivillius phases can be viewed either as consisting of a three-layer oxygen-deficient perovskite slab, $\{Sr_2M'_2M''O_{9.5}\}^{2-}$ (M′ = Nb, Ta, and M″ = Al, Ga), separated by $\{Bi_2O_2\}^{2+}$ sheets, or as consisting of the two-layer Aurivillius phase, $Bi_2SrM'_2O_9$, with an additional oxygen-deficient brownmillerite layer $SrM''O_{2.5}$ inserted into the perovskite layer. As has been observed in some brownmillerite–perovskite intergrowths such as $Sr_3In_2ZrO_8$ and $Ba_3In_2TiO_8$, however, the B cations, M′ and M″, are believed to be disordered within the new three-layer perovskite region.[37]

Attempts to prepare $Bi_2Sr_2Nb_2InO_{11.5}$ and $Bi_2Sr_2Nb_2ScO_{11.5}$ were unsuccessful. This is probably due to the lattice-mismatch strain that develops between the bismuth oxide layer and the perovskite layer because of the larger size of the indium or scandium cation. Indium and scandium can, however, be incorporated into the four-layer Aurivillius phase, $BaBi_4Ti_3M''O_{14.5}$ (M″ = Sc, In, Ga), which we have reported previously.[38] If, as we believe, the M″ cations are randomly distributed within all the perovskite layers,[37,39] then, in a four-layer Aurivillius phase, it should be possible to use larger cations since this would result in a smaller overall increase in the lattice size. This is consistent with what has been observed.

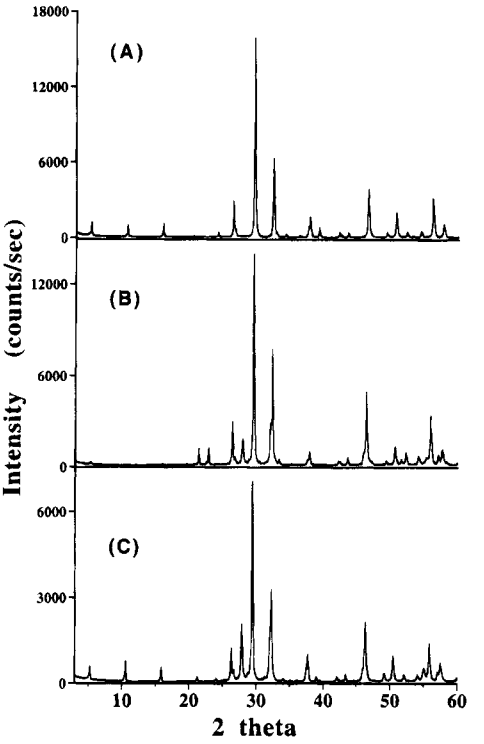

Figure 2. Powder X-ray diffraction pattern of (A) $Bi_2Sr_2Nb_2TiO_{12}$, (B) $Bi_2Sr_2Ta_2GaO_{11.5}$, and (C) $Bi_2Sr_2Nb_2GaO_{11.5}$. The systems were indexed to a tetragonal unit cell.

Table 1. Lattice Constants

compound	a (Å)	c (Å)
$Bi_2Sr_2Nb_2AlO_{11.5}$	3.909(1)	33.26(1)
$Bi_2Sr_2Nb_2GaO_{11.5}$	3.913(1)	33.29(1)
$Bi_2Sr_2Nb_2TiO_{12}$	3.892(1)	33.18(1)
$Bi_2Sr_2Ta_2AlO_{11.5}$	3.904(1)	33.10(1)
$Bi_2Sr_2Ta_2GaO_{11.5}$	3.909(1)	33.20(1)
$Bi_2Sr_2Ta_2TiO_{12}$	3.893(1)	33.13(1)

(b) Powder X-ray Diffraction. The X-ray powder diffraction data, shown in Figure 2 and summarized in Table 1, indicate that all of the compounds are pseudo-tetragonal with lattice parameters that are in agreement with those reported for other three-layer Aurivillius phases.[13] The lattice parameters are also in agreement with recent transmission electron microscopy results obtained for $Bi_2Sr_2Nb_2GaO_{11.5}$.[40] At high values

(27) Gaskell, D. R. *Introduction to Metallurgical Thermodynamics*; Hemisphere Publishing: New York, 1963; pp 223–259.
(28) Reidy, R. F.; Simkovich, G. *Solid State Ionics* **1993**, *62*, 85–97.
(29) Subbarao, E. C. *J. Phys. Chem. Solids* **1962**, *23*, 665–676.
(30) Pham, A.-Q.; Puri, M.; DiCarlo, J.; Jacobson, A. J. *Solid State Ionics* **1994**, *72*, 309–313.
(31) Castro, A.; Millan, P.; Martinez-Lope, M. J. *Solid State Ionics* **1993**, *63–65*, 897–901.
(32) Millan, P.; Castro, A.; Torrance, J. B. *Mater. Res. Bull.* **1993**, *28*, 117–122.
(33) Kikuchi, T. *Mater. Res. Bull.* **1979**, *14*, 1561–1569.
(34) Frit, B.; Mercurio, J. P. *J. Alloys Compounds* **1992**, *188*, 27–35.
(35) Armstrong, R. A.; Newnham, R. E. *Mater. Res. Bull.* **1972**, *7*, 1025–1034.
(36) Kendall, K. R.; Thomas, J. K.; zur Loye, H.-C. *Solid State Ionics* **1994**, *70/71*, 221–224.
(37) Thomas, J. K.; Krause, W. E.; zur Loye, H.-C. In *Materials Research Society Symposium Proceedings: Solid State Ionics*; Nazri, G.-A., Tarascon, J.-M., Armand, M., Eds.; MRS: Boston, MA, 1992; Vol. 293, p 307.
(38) Thomas, J. K.; Kendall, K. R.; zur Loye, H.-C. *Solid State Ionics* **1994**, *70/71*, 225–228.
(39) Thomas, J. K.; Anderson, M. E.; Krause, W. E.; zur Loye, H.-C. In *Materials Research Society Symposium Proceedings: Solid State Ionics*; Nazri, G.-A., Tarascon, J.-M., Armand, M., Eds.; MRS: Boston, MA, 1992; Vol. 293, p 295.

Table 2. Indexing for $Bi_2Sr_2Nb_2AlO_{11.5}$[a]

h	k	l	d_{exp} (Å)	d_{calc} (Å)	I/I_0
0	0	2	16.76	16.63	6.2
0	0	4	8.37	8.31	5.0
0	0	6	5.56	5.54	5.3
0	0	8	4.159	4.157	1.4
1	0	3	3.688	3.686	1.4
1	0	5	3.370	3.370	20.9
0	0	10	3.329	3.326	3.0
1	0	6	3.193	3.194	18.7
1	0	7	3.019	3.019	100.0
1	0	8	2.847	2.848	1.4
1	1	0	2.765	2.764	49.0
1	1	4	2.617	2.623	1.6
1	1	6	2.474	2.474	1.5
1	0	11	2.392	2.391	6.0
0	0	14	2.377	2.375	7.3
1	1	8	2.301	2.302	3.2
1	0	13	2.140	2.141	2.2
0	0	16	2.078	2.079	2.0
2	0	0	1.954	1.954	32.0
0	0	18	1.847	1.848	2.5
1	1	14	1.802	1.802	10.1
1	0	17	1.749	1.749	2.6
2	1	5	1.691	1.691	4.0
2	0	10	1.686	1.685	3.4
2	1	6	1.667	1.667	3.4
2	1	7	1.640	1.641	22.1
1	0	19	1.598	1.597	7.9
1	1	18	1.536	1.536	2.6
2	0	14	1.510	1.509	3.9
1	0	21	1.468	1.468	1.1
2	0	16	1.424	1.424	1.2
2	2	0	1.382	1.382	4.8

[a] Cell parameters of $Bi_2Sr_2Nb_2AlO_{11.5}$ refined to tetragonal unit cell: a = 3.909(1) Å, c = 33.26(1) Å.

of 2θ, however, there appear to be indications of small splittings in some of the reflections, especially in the tantalum compounds, which could suggest the existence of an orthorhombic or monoclinic distortion. Tables 2 and 3 contain the indexing to a tetragonal unit cell for $Bi_2Sr_2Nb_2AlO_{11.5}$ and $Bi_2Sr_2Ta_2AlO_{11.5}$, respectively. In the oxygen-deficient phases, the proposed indexing includes the (106) and the (216) reflections which violate the body-centering conditions. We currently do not understand what structural features are associated with these reflections. In $Bi_2Sr_2Ta_2AlO_{11.5}$, the (216) reflection is not reported because the intensity of the X-ray data at higher angles was weak, and, consequently, it was not possible to accurately determine the peak positions for some of the higher angle peaks. For that reason, also, fewer reflections are reported for $Bi_2Sr_2Ta_2AlO_{11.5}$ than for $Bi_2Sr_2Nb_2AlO_{11.5}$. Figure 3 contains the X-ray powder diffraction pattern for $Bi_2Sr_2Nb_2AlO_{11.5}$ and shows the positions of the indexed peaks.

(c) Conductivity Measurements. Impedance spectroscopy[41,42] was used to determine the ionic conductivity of the samples. The interpretation of the impedance data was made more difficult by the poor resolution between the grain boundary resistance and the bulk resistance. Figure 4 contains impedance spectra for $Bi_2Sr_2Nb_2AlO_{11.5}$ between 400 and 600 °C. The data shown were obtained during the cooling cycle. It is representative of the impedance spectra for all of the materials.

At lower temperatures a single arc was observed in the impedance data (Figure 4c,d) with a spike occurring

Table 3. Indexing for $Bi_2Sr_2Ta_2AlO_{11.5}$[a]

h	k	l	d_{exp} (Å)	d_{calc} (Å)	$I/4I_0$
0	0	2	16.51	16.55	1.5
0	0	6	5.52	5.52	1.4
0	0	8	4.134	4.137	9.7
1	0	1	3.877	3.877	8.5
1	0	5	3.362	3.363	19.4
0	0	10	3.306	3.310	3.4
1	0	6	3.187	3.187	7.1
1	0	7	3.011	3.010	100.0
1	1	0	2.759	2.761	71.7
1	0	9	2.677	2.677	3.2
0	0	14	2.363	2.364	4.8
1	0	13	2.133	2.133	1.4
0	0	16	2.066	2.068	3.5
2	0	0	1.952	1.952	39.8
0	0	18	1.839	1.839	2.9
1	1	14	1.795	1.796	7.6
2	0	8	1.765	1.765	3.3
1	0	17	1.742	1.742	6.6
2	1	5	1.688	1.688	4.9
2	1	7	1.638	1.638	31.4
1	0	19	1.591	1.591	9.2
2	1	9	1.577	1.577	2.2
1	1	8	1.531	1.530	2.6
2	0	14	1.505	1.505	5.2
2	0	16	1.420	1.420	2.8
2	2	0	1.380	1.380	7.5
2	1	15	1.369	1.369	1.2

[a] Cell parameters of $Bi_2Sr_2Ta_2AlO_{11.5}$ refined to tetragonal unit cell: a = 3.904(1) Å, c = 33.10(1) Å.

at lower frequencies. At higher temperatures this spike appeared to form an additional arc (Figure 4a,b), indicating that the electrodes had become nonblocking. Conductivity measurements performed on sample pellets with different geometries (e.g., parallelepiped of dimensions 20 mm × 6 mm × 6 mm) confirmed that this additional arc in the spectra was an artifact of the electrode.

Some of the samples showed separation of the high-frequency arc into multiple arcs, which could be attributed to the bulk and grain resistances; however, this separation was not maintained over any significant temperature range. It was not possible, therefore, to obtain individual resistances by modeling the separated arcs with idealized RC circuits. The use of different sample geometries did indicate that the high-frequency arc was a function of the bulk and grain resistances. Whether additional factors also contributed to the measured resistance is unknown.

All of the conductivity values reported in Table 4, consequently, are based on the sum of the grain and bulk resistances and therefore represent the lower limit for the actual conductivity. The density of the individual pellets (Table 4) that were used for the conductivity measurements was relatively independent of the temperature at which they were sintered. For the pellets with low densities, especially the titanium-containing ones, higher sintering temperatures were ineffective in increasing the density, and decomposition occurred before there was any appreciable increase in density. X-ray data of the pellets after sintering at high temperatures and DTA-TGA data indicated that the samples decomposed between 1250 and 1350 °C. We were also unable to achieve high densities for $Bi_2Sr_2Ta_2AlO_{11.5}$. The powder X-ray data for this sample indicated that the crystallinity was much lower than

(40) Fendorf, M., personal communication, University of California, Berkeley, 1994.

(41) Engstrom, H.; Wang, J. C. *Solid State Ionics* **1980**, *1*, 441–459.

(42) Walter, G. W. *Corros. Sci.* **1986**, *26*, 681–703.

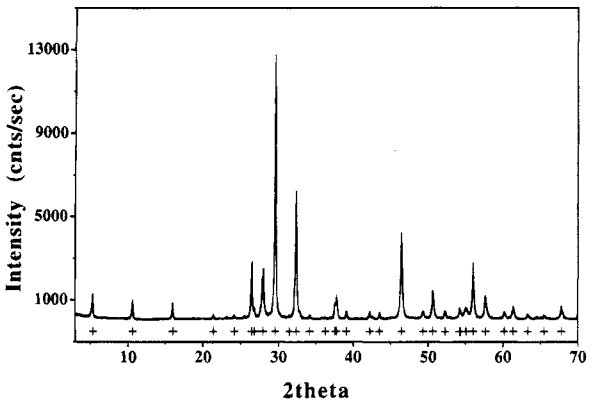

Figure 3. Powder X-ray diffraction pattern of $Bi_2Sr_2Nb_2AlO_{11.5}$. + indicates peak position used in indexing of $Bi_2Sr_2Nb_2AlO_{11.5}$ to a tetragonal unit cell. Calculated verses expected d spacings for this materials are listed in Table 2.

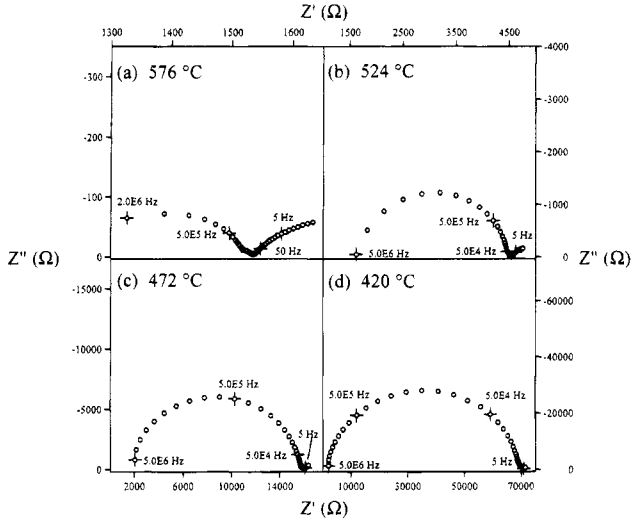

Figure 4. Impedance spectra for $Bi_2Sr_2Nb_2AlO_{11.5}$. The data were obtained during the cooling cycle at (a) 576, (b) 524, (c) 472, and (d) 420 °C. The low-frequency portion of each spectrum on the right, a spike at low temperatures (c, d), an arc at higher temperatures (a, b), represents the electrode contribution. The high-frequency arc on the left represents the total resistance from both the bulk and the grain resistances.

Table 4. Conductivity Measurements[a]

Aurivillius phase	conductivity (S/cm) 900 °C	conductivity (S/cm) 800 °C	activation energy (eV)	density (% theoretical)
$Bi_2Sr_2Nb_2AlO_{11.5}$	2.3×10^{-2}	1.2×10^{-2}	1.26	87
$Bi_2Sr_2Nb_2GaO_{11.5}$	3.6×10^{-2}	2.0×10^{-2}	1.28	93
$Bi_2Sr_2Nb_2TiO_{12}$	1.4×10^{-4}	2.5×10^{-5}	1.91	70
$Bi_2Sr_2Ta_2AlO_{11.5}$	9.2×10^{-4}	4.8×10^{-4}	1.42	68
$Bi_2Sr_2Ta_2GaO_{11.5}$	1.3×10^{-2}	9.3×10^{-3}	1.23	88
$Bi_2Sr_2Ta_2TiO_{12}$	1.8×10^{-5}	3.0×10^{-6}	1.94	62

[a] Conductivity, activation energy, and percent of theoretical density of $Bi_2Sr_2M'_2M''O_{11.5}$ and $Bi_2Sr_2M'_2TiO_{12}$ (M' = Nb, Ta, and M'' = Al, Ga). Activation energy values for oxygen-deficient materials were calculated using the linear portion of Arrhenius plots at low temperatures.

in the other materials, possibly explaining the low pellet density.

The conductivity data for $Bi_2Sr_2Nb_2TiO_{12}$ and $Bi_2Sr_2Ta_2TiO_{12}$, two reference materials that do not contain any oxygen vacancies, are shown in Figure 5 and was linear except for the first several points (below 750 °C), which were slightly elevated relative to later measurements. This higher conductivity during the initial heating cycle was attributed to protonic conduction caused by water adsorbed on the sample. All samples were slightly hygroscopic and, if left in the air for several days, exhibited a minor weight loss when heated. The nonlinearity in the Arrhenius plot of the conductivity disappeared after thermal cycling. The magnitude of the intrinsic conductivity was very low for both of the non-oxygen-deficient samples and exhibited activation energies of almost 2 eV. In the case of $Bi_2Sr_2Nb_2TiO_{12}$, the oxygen partial pressure dependency of the conductivity was measured. The conductivity was inversely related to the pO_2, indicating that the conductivity was due to n-type electronic conduction.[26]

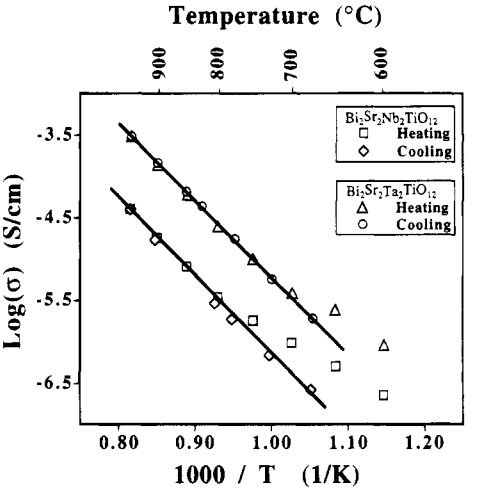

Figure 5. Arrhenius plot of conductivity for $Bi_2Sr_2Nb_2TiO_{12}$ and $Bi_2Sr_2Ta_2TiO_{12}$. The higher conductivity initially is likely due to protonic conduction.

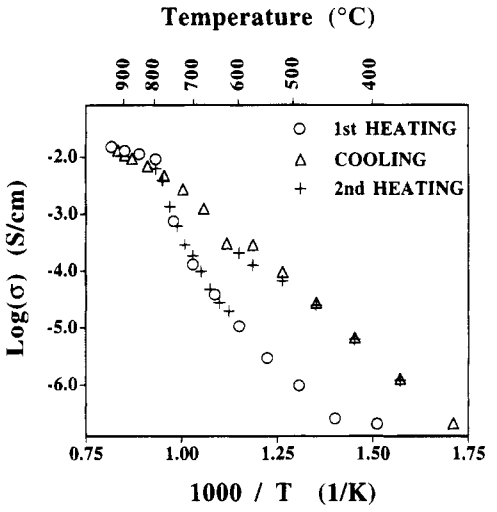

Figure 6. Arrhenius plot of conductivity for $Bi_2Sr_2Ta_2GaO_{11.5}$. The large increase in conductivity during the initial heating cycle occurs between 700 and 800 °C.

The conductivity for both $Bi_2Sr_2Ta_2GaO_{11.5}$ and $Bi_2Sr_2Nb_2GaO_{11.5}$, shown in Figures 6 and 7, respectively, exhibited some very interesting features. The Arrhenius plots of the conductivity data for the initial heating were nonlinear with a jump in the conductivity occurring between 700 and 800 °C. For $Bi_2Sr_2Ta_2GaO_{11.5}$, this represented an increase of over 2 orders of magnitude in the conductivity over a temperature range of only 75 °C. After this jump, the Arrhenius plots became linear, and the activation energy of $Bi_2Sr_2Nb_2GaO_{11.5}$

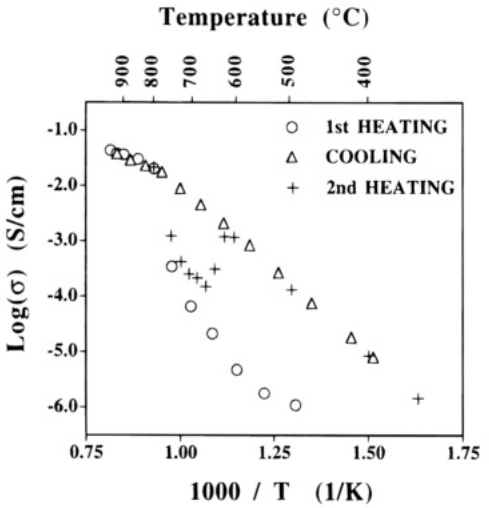

Figure 7. Arrhenius plot of conductivity for $Bi_2Sr_2Nb_2GaO_{11.5}$. The second heating cycle data show a drop in conductivity between 600 and 660 °C.

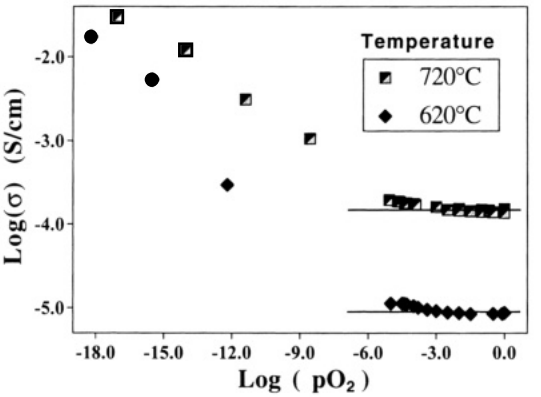

Figure 8. Dependence of conductivity of $Bi_2Sr_2Nb_2GaO_{11.5}$ on oxygen partial pressure. The p_{O_2}-independent region above 10 ppm O_2 indicates predominantly ionic conductivity.

was 0.62 eV. For $Bi_2Sr_2Ta_2GaO_{11.5}$ in the same region the activation energy was 0.46 eV. Upon cooling below 800 °C, both samples again showed a discontinuity in their Arrhenius plots. The conductivity, however, did not decrease to the values seen during the initial heating but instead decreased linearly down to 300 °C. The activation energy for this portion of the plot was 1.28 eV for $Bi_2Sr_2Nb_2GaO_{11.5}$ and 1.23 eV for $Bi_2Sr_2Ta_2GaO_{11.5}$.

The conductivity for these two samples during the second heating cycle was in agreement with the cooling cycle up to 600 °C. Between 595 and 615 °C, however, the conductivity of $Bi_2Sr_2Ta_2GaO_{11.5}$ dropped by an order of magnitude to the value observed during the initial heating cycle. This decrease in conductivity was also observed for $Bi_2Sr_2Nb_2GaO_{11.5}$; however, for this composition the decrease was more gradual and occurred between 600 and 660 °C. Unlike $Bi_2Sr_2Ta_2GaO_{11.5}$, the conductivity of $Bi_2Sr_2Nb_2GaO_{11.5}$ did not fully decrease to the values obtained during the initial heating cycle. Once the conductivities of the two samples stopped decreasing, the conductivities increased in a manner similar to what was observed during the initial heating cycle. By 800 °C, the conductivities for $Bi_2Sr_2Nb_2GaO_{11.5}$ and $Bi_2Sr_2Ta_2GaO_{11.5}$ during the second heating cycle coincide with both the initial heating and cooling cycles. It appears that once $Bi_2Sr_2Nb_2GaO_{11.5}$ and $Bi_2Sr_2Ta_2GaO_{11.5}$ are cooled below a certain temperature, a more conductive low-temperature phase becomes metastable. When the sample is heated up again, the sample undergoes a transition back to a less conductive state. The conductivity values do not, however, necessarily descend all the way down to the values obtained during the initial heating cycle.

The portion of the conductivity due to ionic conduction for $Bi_2Sr_2Nb_2GaO_{11.5}$ at 620 and 720 °C and for $Bi_2Sr_2Ta_2GaO_{11.5}$ at 720 °C was determined by measuring the dependence of the conductivity on the partial pressure of oxygen. For p_{O_2} down to 10 ppm, at both 620 and 720 °C, the conductivity of $Bi_2Sr_2Nb_2GaO_{11.5}$ increased only slightly. As the p_{O_2} decreased further, the conductivity began to increase more quickly. The behavior observed at lower oxygen concentrations is representative of a mixed ionic conductor with n-type conduction.[28,43,44] From the plot of conductivity as a function of p_{O_2}, as shown in Figure 8, we can conclude that the electronic contribution to the total conductivity is minimal for oxygen partial pressures greater than 10 ppm. The conductivity of $Bi_2Sr_2Ta_2GaO_{11.5}$ was also independent of the oxygen partial pressure for p_{O_2} greater than 10 ppm. A concern with bismuth-containing compounds is the stability of the materials under reducing atmospheres. This is one of the problems with using bismuth oxide as an ionic conductor. From the reproducibility of the conductivity data as a function of partial pressure and from X-ray data after completion of the dependency measurements, it appears that at the temperatures measured, $Bi_2Sr_2Nb_2GaO_{11.5}$ is not degraded by partial pressures of oxygen down to 10^{-18} atm. $Bi_2Sr_2Ta_2GaO_{11.5}$, however, does decompose between 10^{-6} and 10^{-9} atm of oxygen.

The initial conductivity data that are observed for $Bi_2Sr_2Nb_2AlO_{11.5}$ is dependent upon the final thermal cooling rate during sample preparation. If the sample is cooled slowly, the conductivity will be similar to the conductivity of the sample after it has undergone the first heating and cooling measurement cycle. The Arrhenius plot of the conductivity increases in a linear manner; however, the more conductive state exhibits instability relative to the less conductive state as the temperature is increased. We believe that this is related to what is observed in $Bi_2Sr_2Ta_2GaO_{11.5}$ and $Bi_2Sr_2Nb_2GaO_{11.5}$. $Bi_2Sr_2Nb_2AlO_{11.5}$ can remain in the more conductive state at room temperatures for prolonged periods of time. It will, however, begin to return to the less conductive state as it is heated up. Once the temperature reaches 825 °C, the values for the conductivity coincide with the values shown in Figure 9.

The data for Figure 9 were obtained by rapidly cooling $Bi_2Sr_2Nb_2AlO_{11.5}$ to room temperature. In this way, it was possible to obtain the conductivity phase that was observed during the initial heating cycle for all of the other ionic conductors. The difference in the magnitude of the conductivity between the two low-temperature states is much less than in the two gallium-containing samples. This supports the idea that in $Bi_2Sr_2Nb_2AlO_{11.5}$ there is a much smaller energy difference between the two low-temperature states and that it is, therefore, easier to access the more conductive state at lower temperatures. The activation energy of the more

(43) Ling, S.; Anderson, M. P.; Ramanarayanan, T. A. *Solid State Ionics* **1993**, *59*, 33–45.
(44) Maier, J. *Angew. Chem., Int. Ed. Engl.* **1993**, *32*, 313–335.

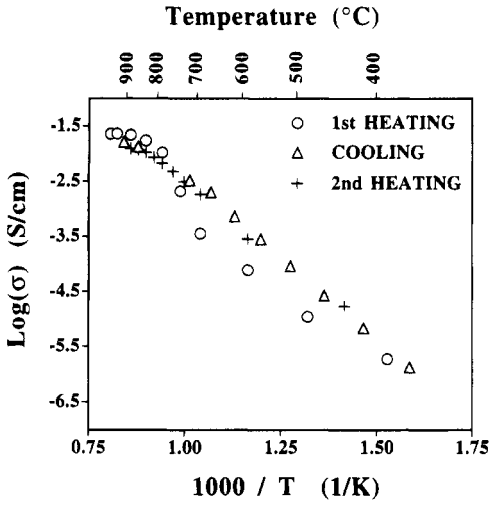

Figure 9. Arrhenius plot of conductivity for $Bi_2Sr_2Nb_2AlO_{11.5}$. Data obtained after cooling from 850 °C at 10 °C/min. This cooling rate stabilized the lower conductive state.

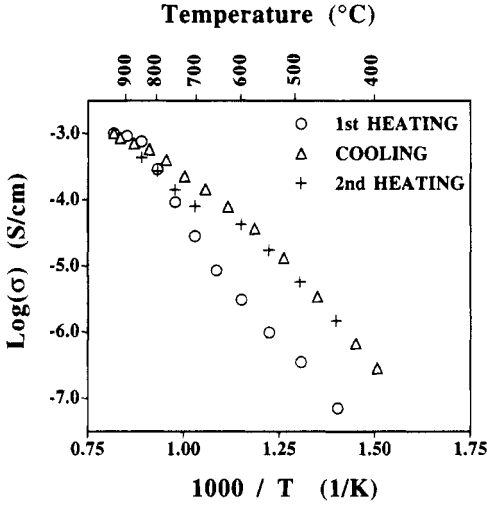

Figure 10. Arrhenius plot of conductivity for $Bi_2Sr_2Ta_2AlO_{11.5}$. The magnitude of conductivity is much lower than in other oxygen-deficient materials.

conductive state was 1.26 eV, which is similar to that observed for the $Bi_2Sr_2Nb_2GaO_{11.5}$ (1.28 eV).

The conductivity for $Bi_2Sr_2Ta_2AlO_{11.5}$ is shown in Figure 10 and was much lower than that measured for any of the other oxygen-deficient structures. Several possible explanations exist for the lower conductivity. These include (1) low pellet density, (2) poor crystallinity as evidenced by lower peak intensities and peak broadening in the X-ray data, and (3) higher energy required for oxygen transport. Because we were unable to separate the bulk and grain resistance in the impedance data, we could not ascertain the exact cause for the lower conductivity. It appears, however, that multiple conductivity states exist in $Bi_2Sr_2Ta_2AlO_{11.5}$, as confirmed by the Arrhenius plot of the conductivity. Also, the activation energy of 1.42 eV, which is close to that of the other oxygen-deficient materials, suggests that the transport mechanism is similar.

(d) Differential Thermal Analysis. The observed discontinuities in these ionic conductors are believed to be due to the disordering of the oxygen vacancies.[23] Consequently, we examined all of the samples by DTA-TGA to look for evidence of these order–disorder transitions believed to accompany the jumps in the ionic

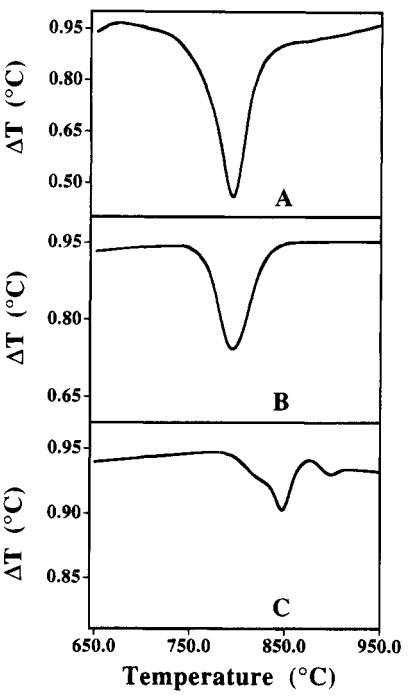

Figure 11. DTA data for (A) $Bi_2Sr_2Nb_2GaO_{11.5}$, (B) $Bi_2Sr_2Ta_2GaO_{11.5}$, and (C) $Bi_2Sr_2Nb_2AlO_{11.5}$, showing endothermic peaks associated with order/disorder transitions in the oxygen vacancies.

conductivity. The DTA-TGA data obtained in air for $Bi_2Sr_2Nb_2TiO_{12}$ and $Bi_2Sr_2Ta_2TiO_{12}$, neither of which contain oxygen vacancies, did not indicate any phase transition or weight loss between 300 and 1200 °C. $Bi_2Sr_2Nb_2GaO_{11.5}$, on the other hand, showed a very large endothermic transition (Figure 11A) starting at 760 °C and peaking at 795 °C. This transition coincides with the discontinuity that occurs in the Arrhenius plot and could explain the large jump in conductivity. $Bi_2Sr_2Ta_2GaO_{11.5}$ also displays a single endothermic peak (Figure 11B) in the DTA data, with an onset at 756 °C and a peak at 791 °C, again coinciding with the observed jump in the conductivity data. The endothermic peak observed for $Bi_2Sr_2Nb_2AlO_{11.5}$ is very weak (Figure 11C) and appears to be the result of more than one phase transition. The peak is spread out between 771 and 843 °C, and the nature of the additional transitions is presently not known. The DTA-TGA data, however, do agree with the conductivity data in that we did not observe a sharp transition but rather a gradual change. $Bi_2Sr_2Ta_2AlO_{11.5}$ did not show any phase transition that we were able to detect by DTA. Whether the inability to detect any phase transitions was because of their absence in the material or because the transitions were so weak as to be below the resolution of our simultaneous DTA-TGA is unknown.

(e) Mechanism. In trying to synthesize and characterize new ionic conductors, we have come upon a system that appears to undergo very interesting structural changes that directly affect the conductivity of the sample. We believe that the oxygen vacancies in the perovskite layers undergo an order–disorder transition and that this greatly increases the ionic conductivity. This type of transition has been observed in the brownmillerite structure ($Ba_2In_2O_5$),[22,45] in perovskite/brownmillerite intergrowths ($Ba_3In_2TiO_8$),[38] and in other oxygen-deficient Aurivillius phases ($BaBi_4Ti_3ScO_{14.5}$,

$Bi_2NaNb_2O_{6.5}$).[30,37] The vacancy-disordered state remains stable below the initial onset temperature upon subsequent cooling. This behavior has been observed before in the four-layer Aurivillius-like phases;[38] however, for the new materials reported in this paper, the disordered state remains stable down to 300 °C, and in the case of $Bi_2Sr_2Nb_2AlO_{11.5}$, the higher conductive state can remain stable even at room temperatures. This suggests that there is a kinetic component to the transition and that multiple phases can exist at specific temperatures, depending upon the thermal history of the sample.

As these new materials are heated above a transition temperature, the oxygen vacancies in the perovskite layer are believed to become dissociated from the trivalent cations, either aluminum or gallium. The vacancies, consequently, become disordered over the entire perovskite layer. This is comparable to what occurs in brownmillerite material such as $Sr_2Fe_2O_5$, where above a transition temperature (700 °C) the material transforms from the brownmillerite structure (ordered oxygen vacancies) into a perovskite-like structure in which the oxygen vacancies are randomized over all oxygen positions.[46] The randomization or disorder of the oxygen vacancies results in a decrease in the energy required for the oxygen to hop from an occupied lattice site to an unoccupied site and, consequently, increases the ionic conductivity.

When the new materials that we have synthesized are cooled below a specific transition temperature, the oxygen vacancies begin to reorder. They do not, however, become completely reassociated with the trivalent cation as evidenced by the higher than expected conductivity. A similar partial reordering has been suggested in work done on the energetics of the order–disorder transition and on the oxygen dynamics of $Ba_2In_2O_5$.[45,47] In that case the order–disorder transition, which occurred at 932 °C, was found not to involve all of the oxygen vacancies. It also implied the possible existence of continued short-range ordering even at high temperatures. If partial ordering exists in these oxygen-deficient materials, then the transition observed on cooling would be representative of a transformation not necessarily from a completely disordered system to a completely ordered system but rather from a partially disordered system to another partially disordered system. For presumably kinetic reasons the vacancies are prevented from completely ordering. As the material is cooled further, some form of strain develops in the material. If the materials are then reheated above a critical temperature or cooled to room temperature, the vacancies will fully order. This fully ordered state is what is observed during the initial heating cycle.

Further study into the structure of these new materials and the observed phase transitions using high-temperature X-ray and neutron diffraction is planned to better understand the mechanism of the oxygen ion conductivity. We also plan to explore the ionic conductivity in two-, three-, and four-layer Aurivillius-like systems that contain different concentrations of oxygen vacancies.

Acknowledgment. The authors wish to thank Carlos Navas for help with the $Bi_2Sr_2Ta_2GaO_{11.5}$ sample. They would also like to thank the National Science Foundation for support of this research through grant DMR-9200688. J.K.T. would like to thank A. D. Little and AT&T Bell Laboratories for support.

CM940277W

(45) Adler, S. B.; Reimer, J. A.; Baltisberger, J.; Werner, U. *J. Am. Chem. Soc.* **1994**, *116*, 675–681.
(46) Shin, S.; Yonemura, M.; Ikawa, H. *Mater. Res. Bull.* **1978**, *13*, 1017–1021.
(47) Prasanna, T. R. S.; Navrotsky, A. *J. Mater. Res.* **1993**, *8*, 1484–1486.